

Modeling the influence of hydroperiod and vegetation on the cross-sectional formation of tidal channels

Andrea D'Alpaos^{a,*}, Stefano Lanzoni^a, Simon Marius Mudd^b, Sergio Fagherazzi^c

^a *Dipartimento di Ingegneria Idraulica, Marittima Ambientale e Geotecnica and International Centre for Hydrology "Dino Tonini", University of Padova, Italy*

^b *Department of Civil and Environmental Engineering, Vanderbilt University, Nashville, TN, USA*

^c *Department of Geological Sciences and School of Computational Science, Florida State University, Tallahassee, FL, USA*

Received 6 April 2006; accepted 2 May 2006

Available online 11 July 2006

Abstract

The evolution of the cross section of a salt-marsh channel is explored using a numerical model. Deposition on the marsh platform and erosion and deposition in the channel affect the tidal prism flowing through the cross section, such that the model captures the evolution of the stage–discharge relationship as the channel and marsh platform evolve. The model also captures the growth of salt-marsh vegetation on the marsh platform, and how this vegetation affects flow resistance and the rate of sedimentation. The model is utilized to study the influence of hydroperiod and vegetation encroachment on channel cross section. Numerical results show that a reduction in hydroperiod due to the emergence of the marsh platform causes an infilling of the channel. Vegetation encroachment on the marsh surface produces an increase in flow resistance and accretion due to organic and mineral sedimentation, with important consequences for the shape of the channel cross section. Finally, modeling results indicate that in microtidal marshes with vegetation dominated by *Spartina alterniflora*, the width-to-depth ratio of the channels decreases when the tidal flats evolve in salt marshes, whereas the cross-sectional area remains proportional to the tidal peak discharge throughout channel evolution.

© 2006 Elsevier Ltd. All rights reserved.

Keywords: tidal channel; salt-marsh vegetation; tidal flats; hydroperiod; coastal geomorphology

1. Introduction

Salt marshes are common in intertidal zones, and are composed of platforms dissected by a network of tidal creeks that transport both water and sediment onto and away from a vegetated surface populated by a limited number of macrophyte species such as *Spartina alterniflora* and *Juncus roemerianus*. The hydrodynamics of these environments depends on the structure and density of tidal creeks (e.g., Fagherazzi et al., 1999; Rinaldo et al., 1999a,b; Marani et al., 2003), while sedimentation rates vary as a function of the distance from

the channel, thus linking sediment transport processes to network morphology and drainage density (e.g., Christiansen et al., 2000; Leonard et al., 2002; Temmerman et al., 2003a,b). Similarly, the composition and distribution of salt-marsh macrophytes depends on the characteristics of the channel network since they play an important role in several edaphic factors, such as nutrient fluxes and soil salinity (Sanderson et al., 2000).

A number of authors have studied the strictly intertwined nature of salt marshes and tidal channels cutting through them. Several models have been proposed to investigate the zero-dimensional growth of salt marshes, where the sedimentation on the marsh platform is a function of sediment supply and either marsh elevation (e.g., Krone, 1987; French, 1993; Allen, 1994, 1995, 1997; Temmerman et al., 2003a) or

* Corresponding author.

E-mail address: adalpaos@idra.unipd.it (A. D'Alpaos).

biomass (Randerson, 1979; Morris et al., 2002). The differential accretion of the marsh platforms, induced by the spatial variability of sediment deposition rates, as a function of the distance from the creek, has also been analyzed (Woolnough et al., 1995; Mudd et al., 2004; Temmerman et al., 2004). The development of tidal channels and, more generally, the morphodynamics of tidal networks, have been explored both in the field (e.g., Pestrong, 1965; Gardner and Bohn, 1980; Steel and Pye, 1997) and with conceptual and numerical models (e.g., Yapp et al., 1916, 1917; Beeftink, 1966; French and Stoddart, 1992; French, 1993; Allen, 2000; Fagherazzi and Furbish, 2001; Fagherazzi and Sun, 2004; D'Alpaos et al., 2005). In general, the evolution of a tidal creek is enhanced by small perturbations in the topography on an antecedent surface subject to tidal fluxes, which could be a mud flat or a terrestrial region that is being encroached by salt water due to sea-level rise (e.g., Allen, 2000; Gardner and Porter, 2001). As perturbations grow, water flow concentrates within the incipient channel, favoring an increase of the shear stresses and, therefore, erosion within the channel, which widens and deepens (Steel and Pye, 1997). However, a feedback mechanism exists which relates the time evolution of cross-sectional geometry (Friedrichs, 1995; Fagherazzi and Furbish, 2001) to the vertical growth of the salt-marsh platform, which tends to reduce the tidal prism and, as a consequence, enhances channel infilling. The flow velocity and shear stress distribution within tidal channels are, in fact, determined in large part by the size of the tidal prism which flows into and out of the intertidal zone (e.g., Pethick, 1980; Allen, 2000).

Field investigators have noted that the above evolutionary scenario is strongly influenced by the presence of vegetation which affects not only the planimetric evolution of tidal channels (e.g., Garofalo, 1980; Gabet, 1998) but also flow characteristics (e.g., Kadlec, 1990; Leonard and Luther, 1995; Nepf, 1999; Mudd et al., 2004) and sedimentation processes (e.g., Gleason et al., 1979; Randerson, 1979; Yang, 1998; Leonard et al., 2002; Morris et al., 2002). For example, the rate at which water can propagate onto and drain from the platform adjacent to a channel is influenced by the drag caused by the stems of macrophytes living upon it (Nepf, 1999), which increases linearly with plant density (Lopez and Garcia, 2001). As a direct consequence, flow speed in the marsh canopy is inversely related to stem density so that the volume of water transported as a sheet flow on the marsh platform considerably decreases when vegetation is present (Leonard and Luther, 1995). Vegetation also favors particle settling and consequent platform accretion by a reduction of turbulence levels within the canopy (Leonard and Luther, 1995; Christiansen et al., 2000). However, these studies do not investigate the response of unvegetated tidal channel cross sections to vegetation encroachment on the marsh platform.

In this paper, we focus on the long-term evolution of the channel cross section, starting from the initial channel formation within a tidal flat, with particular emphasis to the role played by hydroperiod and vegetation. In order to investigate the driving factors which lead to the observed cross-sectional

geometry, we track the growth of the emergent marsh platform coupled to the evolving morphology of the tidal channel. To this end, we extend the analysis of Fagherazzi and Furbish (2001), by considering water levels and flow discharges variable in time, resulting from a quasi-static propagation of the tide within a given intertidal area, and accounting for the reduction of the tidal prism after the emergence of the marsh surface, and for the effects of vegetation on surface drag and sediment deposition. Furthermore we assume a constant value for the suspended sediment concentration across the section which bears as consequence that the deposition of sediments at the surface is directly proportional to the hydroperiod.

The new model can then follow the time evolution of tidal channels, not only on youthful marshes like those studied by Fagherazzi and Furbish (2001), but also at late stages of marsh evolution, when the marsh is emergent. In order to quantify the effects of vegetation encroachment on channel cross section we consider the case of a particular species of macrophytes, *Spartina alterniflora*, using the empirical data gathered from North Inlet Estuary, South Carolina (Morris and Haskin, 1990; Morris et al., 2002), and the approach of Mudd et al. (2004) and Palmer et al. (2004) to model the influence of such a species on tidal flow and sedimentation. The data will be used to determine the model parameters.

A series of two simulations are presented. The first set of simulations analyzes the influence that marsh-platform vertical accretion and channel cross-sectional evolution exert on each other, and how the hydroperiod and, therefore, the final cross-sectional configuration are affected by this intertwined interaction. Inorganic sediment deposition is modeled as a linear function of the hydroperiod, following the zero-dimensional formulation of a number of authors (e.g., Krone, 1987; Woolnough et al., 1995; Allen, 1997). In the second set of simulations, we take into account the role exerted by *Spartina alterniflora* on the sedimentation rate on the platform as a function of the biomass of the macrophytes on the marsh following the approach of Mudd et al. (2004). The influence of vegetation encroachment on channel cross-sectional shape is therefore analyzed and discussed.

The paper is organized as follows: in Section 2 we describe the methods used to build the model and its structure, the assumptions adopted to describe the hydrodynamics, sediment transport processes, and the effect of vegetation. Section 3 then presents the main results obtained by applying the model under different scenarios. A discussion section where we compare significant geomorphic features of the modeled cross sections to the ones of observed tidal channels and a set of conclusions close the paper.

2. Methods

2.1. The hydrodynamic model

We analyze the morphodynamic evolution of a generic cross section composed of a tidal channel and an adjacent marsh platform (e.g., the transect *B–C* shown in Fig. 1) which drains a sub-basin of area *A*, whose extent can be determined

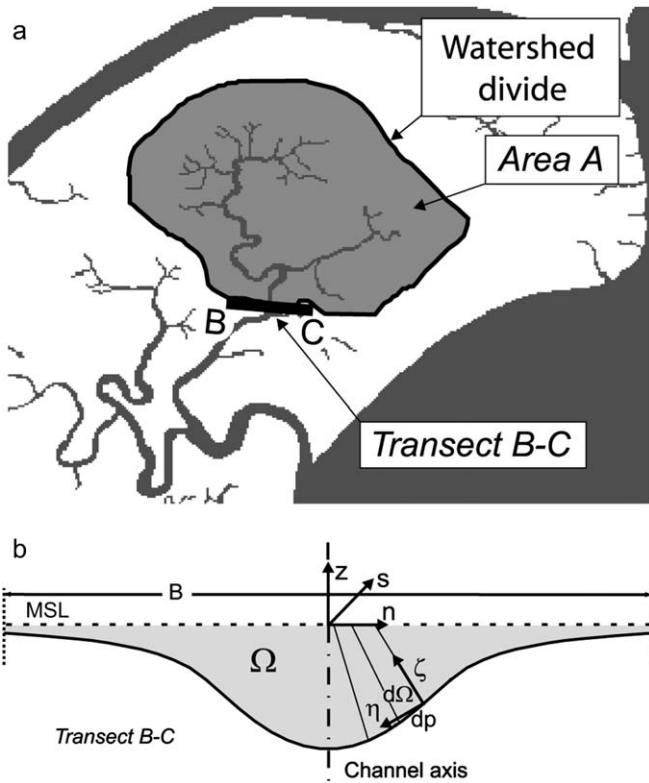


Fig. 1. (a) Portion of the tidal basin (in gray) drained by the considered cross section (B–C). The tidal watershed of area A and its divide is delineated by using the procedure proposed by Rinaldo et al. (1999a) and are delineated by Marani et al. (2003); (b) typical salt-marsh cross-sectional configuration investigated through the model and notation. The origin of the n, s, z coordinate system is located at the intersection of channel axis and the mean sea level (MSL, which is assumed equal to 0). Note that the spacing between normals to the bottom is greatly exaggerated.

through the procedure proposed by Rinaldo et al. (1999a) and refined by Marani et al. (2003). We assume that the initial bottom configuration of the sub-basin is characterized by a nearly flat surface, with an average elevation well below the minimum low water level (MLWL). For the sake of simplicity, we also assume that the tidal sub-basin has a rectangular shape, and is characterized by a width B and by an upstream length L . The bidimensional model proposed by Fagherazzi and Furbish (2001) simulates the evolution in time of any tidal-flat or salt-marsh transect for given values of the water level and of the flow discharge. In the present contribution we relax such an assumption by considering time varying water levels and flow discharges, resulting from a quasi-static propagation of the tide within the area A closed by the reference cross section under investigation (Fig. 1). At every instant t of the tidal cycle, the discharge flowing through the transect B–C is then calculated following the static model introduced by Boon (1975) and Pethick (1980):

$$Q(t) = \frac{dV}{dt} = \frac{d}{dt}[A(t)D_0(t)] \quad (1)$$

where $A(t)$ is the time-dependent liquid (horizontal) area of the intertidal surface drained by the considered cross section, $V(t)$

is the instantaneous volume of water over the intertidal surface, $D_0(t)$ is the instantaneous mean water depth over the cross section, calculated as $h(t) - z_b(t)$, with $h(t)$ and $z_b(t)$ the instantaneous water and mean bottom elevations over a reference datum, respectively. It is important to note that the drainage area, $A(t)$, is equal to the entire intertidal area (BL) drained by the considered cross section when the domain is completely inundated, but it reduces to its submerged portion ($B_{wet}L$, where B_{wet} denotes the width of the wetted portion of the transect) when part of the intertidal surface emerges. In our simplified approach, in fact, we do not account for water volume variations related to either the upstream funneling of the channel section and the longitudinal gradients of marsh surface elevation. Such an assumption is justified by the fact that, usually, the convergence length of tidal creeks tends to be larger than the length of the tidal sub-basin (Marani et al., 2002) and that the landward bottom aggradation of the areas flanking the channel is quite small.

At each time step, the oscillating discharge calculated through Eq. (1) is used to evaluate the repartition of bottom shear stresses. Following the procedure introduced by Pizzuto (1990) in the context of gravel rivers, the local value of the bottom shear stress, τ_0 , reads:

$$\tau_0 = \rho g S \frac{d\Omega}{dp} + \frac{d}{dp} \int_0^{D_\zeta} \tau_{\zeta s} d\zeta \quad (2)$$

where ρ is the water density, g is the gravitational acceleration, S is the energy slope, $d\Omega$ the cross-sectional area between two normals to the bed, dp is the wetted perimeter related to $d\Omega$, ζ is a local spatial coordinate normal to the bottom, D_ζ is the total distance along ζ from the bed to the water surface, and $\tau_{\zeta s}$ is the bottom shear stress acting on planes orthogonal to ζ and directed seawards (see Fig. 1b for notation). For details on how Eq. (2) was derived and utilized to model the cross-sectional evolution of salt-marsh channels see Pizzuto (1990) and Fagherazzi and Furbish (2001).

Boundary conditions need to be carefully specified in order to solve Eq. (2). When the entire cross section is unvegetated, the velocity profile along the normal, introduced in order to evaluate $\tau_{\zeta s}$, can be assumed to be logarithmic. Two (identical, for symmetry reasons) boundary conditions are then imposed at the two ends of the transect, associated with the watershed divides, delimiting the drainage area, A (see Fig. 1b), namely:

$$\tau_0 = \rho g S D \quad n = \pm B/2 \quad (3)$$

where D is the local water depth. Note that such boundary conditions have very little effect on the overall stress distribution over B during the cross-sectional evolution, even though they influence the stress near $n = \pm B/2$.

The assumption of a logarithmic velocity distribution along the normal to the bottom, ζ , does not apply when the marsh surface becomes vegetated. As clearly demonstrated by field measurements and experiments carried out by Leonard and Luther (1995) and by Nepf and Vivoni (2000), the velocity

distribution is strongly affected by the presence of vegetation, and a logarithmic profile is likely to be attained only above the canopy.

Therefore, Eq. (2) can be applied only on the unvegetated portions of the cross-section, which are basically located in the deeper central part, considering a reduced value of the flow discharge. We then impose the boundary conditions (3) on τ_0 , at the edge between the vegetated and unvegetated area, rather than at the endpoints of the transect. The shear stresses on the vegetated portion of the cross section, which are used uniquely to estimate the erosion/deposition rates, are evaluated by retaining only the first term on the right hand side of Eq. (2).

Indeed, the second term on the right hand side of Eq. (2), which is responsible for momentum redistribution, has little effect on the shear stress spatial distribution when the bed is nearly horizontal, as on the marsh platform.

In order to account for the discharge redistribution which occurs as soon as vegetation starts to encroach the marsh surface, the discharges flowing, respectively, through the central unvegetated part of the transect and through the rougher vegetated portions of the cross-section, are calculated by using the procedure proposed by Engelund (1966). In particular, in the presence of vegetation, the friction coefficient to be used in the Darcy-Weisbach flow resistance relationship can be evaluated by considering the results of recent experimental studies by Nepf (1999), relating the bulk plant drag coefficient to the product of the projected plant area per unit volume, a_s , and the stem diameter, d_s , which, as it will be discussed later, can be easily related to plant biomass (Mudd et al., 2004).

The bulk drag coefficient, c_D , can then be written as:

$$c_D = \alpha_{c_D} b + c_{D0} \quad (4)$$

where c_{D0} is the drag coefficient without vegetation, b is the biomass and α_{c_D} is a fitting parameter which links the biomass to the drag coefficient (Mudd et al., 2004). The one-dimensional balance between gravity and drag forces allows one to obtain the friction coefficient, f , which has to be used in the Darcy-Weisbach flow resistance relationship, namely:

$$f = 4c_D a_s D \quad (5)$$

where a_s is the projected plant area per unit volume, and D is the local water depth.

Finally, we note that, at a given instant, the energy slope S appearing in Eq. (2), is calculated iteratively, by imposing that the total discharge flowing through the transect equals Q . We start with a guessed value of S , compute the shear stress and flow velocity distributions, we then calculate the corresponding discharge Q , if it is higher (lower) than the actual value (determined through Eq. (1)) we reduce (increase) S until convergence (see also Fagherazzi and Furbish, 2001). This is an approximation because actual velocities, energy slope and water depth are related together through the continuity and momentum equations. However, our aim is not to fully describe the flow field caused by tidal motion within an intertidal cross-sectional area, but rather to provide a simplified

geomorphological model able to capture the main features of the cross-sectional evolution of tidal channels.

2.2. Sediment erosion and deposition

We assume the bottom sediment to be cohesive, an assumption consistent with field observations. Evolution of bed topography is governed by the sediment continuity equation which can be written in the form:

$$(1 - \lambda) \frac{\partial z_b}{\partial t} = Q_d - Q_e \quad (6)$$

where z_b is the bottom elevation, λ is void fraction in the bed, and Q_d and Q_e are the deposition and the erosion fluxes, respectively, representing sediment mass exchange rates, per unit area, between the water column and the bed.

Many mathematical formulations have been proposed for Q_d and Q_e . Here a formulation which can be applied when the bed properties are relatively uniform over the depth and the bed is consolidated (Mehta, 1984) is used:

$$Q_e = Q_{e0} \frac{\tau_0 - \tau_c}{\tau_c}, \quad \tau_0 > \tau_c \quad (7)$$

where τ_0 is the local value of the bottom shear stress evaluated through Eq. (2), τ_c is the cohesive shear stress strength with respect to erosion, and Q_{e0} is a constant empirical erosion rate which depends on sediment properties.

As far as the deposition rate is concerned, various sedimentation mechanisms have to be considered, namely:

$$Q_d = Q_{ds} + Q_{dt} + Q_{db} \quad (8)$$

where Q_{ds} is the deposition rate due to settling, Q_{dt} is the sedimentation rate due to the trapping effect of the plant canopy, and Q_{db} is the belowground net organic production due to plant roots and rhizomes. If the marsh is not vegetated, both sediment trapping and below ground organic production are identically zero.

The deposition due to particle settling acts even without the presence of vegetation and is the chief process responsible for marsh accretion. To estimate Q_{ds} , the model uses the formulation of Einstein and Krone (1962):

$$Q_{ds} = w_s C_b \left(1 - \frac{\tau_0}{\tau_d} \right), \quad \tau_0 < \tau_d \quad (9)$$

where w_s is the settling velocity that depends on the size of the estuarine sediment flocs (Gibbs, 1985), τ_d is the shear stress below which all initially suspended sediment eventually deposits, C_b is the volumetric sediment concentration at the bottom, which, following Parker et al. (1987), can be written as $C_b = rC_0$, with r an empiric coefficient ($r \cong 2$), and C_0 the depth-averaged volumetric concentration of sediments in the water column.

We consider a bottom composed of fine sediment, which is transported mainly in suspension. The values typically attained across the section by the Rouse number ($Z = w_s k^{-1} u_*^{-1}$, with k

the von Karman constant, and u_* the friction velocity) are small enough ($\cong 0.02$ in our simulations) to assume that the sediment is well mixed across the water column. Moreover, the ratio of the horizontal to the vertical length scale is quite large, thus ensuring that the horizontal diffusion of sediment can be neglected with respect to the horizontal advection.

Mathematical modeling of suspended sediment transport carried out by Pritchard and Hogg (2003) indicates that, away from the shoreline, the depth-averaged concentration of suspended sediment tends to a constant value which, generally, is a function of the threshold velocities for erosion and deposition. In our simulations we then assume that the suspended sediment concentration in the water column is constant across the section and throughout the simulation. Note that this assumption is widely utilized in zero-dimensional models that focus on the interplay between salt-marsh accretion and sea-level rise (Krone, 1987; Allen, 1994). Moreover, with the assumption of constant sediment concentration, the deposition of sediments at the surface is directly proportional to the hydroperiod, so that for mature marshes the rate of marsh accretion decreases and the marsh elevation tends toward an asymptotic value that corresponds to mean high tide (Pethick, 1981).

For emergent salt marshes the vegetation encroachment at the surface increases the amount of sediment deposited due to the trapping effect of plant stems and leaves and the reduction of turbulence due to vegetation. Nepf (1999) demonstrated the reduction in turbulence caused by plant stems using laboratory experiments. Leonard and Luther (1995) and Leonard et al. (2002) found that turbulent energy within vegetated canopies on marsh platforms were much smaller than the turbulent energies in marsh creeks. Others have found turbulence to be a primary influence of sediment transport in intertidal areas (e.g., French et al., 1993).

The above studies suggest that the amount of sediment trapped is proportional to the concentration of suspended sediment and to the number of plant stems that can both reduce the turbulent energy and capture sediment particles. Following Palmer et al. (2004), we express the trapping rate as follows:

$$Q_{dt} = C_0 u \eta d_s n_s h_s \quad (10)$$

where u is a typical value of the flow speed through vegetation, η is the rate at which transported sediment particles are captured by plant stems, d_s is the stem diameter, n_s is the stem density per unit area, and h_s is the average height of the stems. The capture efficiency η reads:

$$\eta = \alpha_\eta \left(\frac{u d_s}{\nu} \right)^{\beta_\eta} \left(\frac{d_p}{d_s} \right)^{\gamma_\eta} \quad (11)$$

where d_p is particle diameter, ν is the kinematic viscosity of the water, α_η , β_η , and γ_η are empirical coefficients obtained by Palmer et al. (2004).

Finally, the belowground production of organic matter can be directly linked to the biomass following the work of Randerson (1979):

$$Q_{db} = Q_{db0} \frac{b}{b_{\max}} \quad (12)$$

where b_{\max} is the maximum value of the biomass, and Q_{db0} is a typical deposition rate which is derived empirically from field measurements. For example Blum and Christian (2004), report a maximum organic sediment accretion of about 9 mm/year for a *Spartina alterniflora* marsh in Virginia. In reality the belowground storage of organic material in salt marshes is an extremely complex process that involves root production, microbial decomposition, as well as edaphic factors such as nutrients availability and salinity (Blum and Christian, 2004; Cahoon et al., 2004) which are not considered in our simplified approach.

2.3. Vegetation parameterization

Eqs. (4), (5), (10)–(12) require the estimate of plant biomass, b , as well as of several parameters related to it as: η , d_s , n_s , h_s , Q_{db0} and b_{\max} . In the present contribution we focus on the case of salt marshes characterized by a prevailing presence of *Spartina alterniflora*, a species of halophytic vegetation quite common in tidal environments. Long-term field studies on the physiology of a *S. alterniflora* community at North Inlet estuary, South Carolina, have been carried out by Morris and Haskin (1990) and Morris et al. (2002). The observed data show that the biomass of *S. alterniflora* can be related (Mudd et al., 2004) to the differences $z_{\max} - z_b$ and $z_{\max} - z_{\min}$, where z_{\max} is the maximum elevation withstood by *S. alterniflora*, z_{\min} is the minimum value at which vegetation starts to encroach the surface, and z_b is the local marsh elevation. The duration of inundation, in fact, will decrease as z_b increases, thus affecting soil salinity because evapotranspiration concentrates salts in pore water if the marsh is not regularly flooded (Morris, 1995). A number of researchers have shown that increased pore water salinity caused by evapotranspiration can limit growth or be fatal to salt-marsh macrophytes (e.g., Phleger, 1971; Webb, 1983; Morris, 2000). While other biotic and abiotic factors may be important in determining plant productivity (see Silvestri and Marani, 2004, and references therein), following the approach adopted by Mudd et al. (2004), based on the long record of plant productivity at North Inlet, we relate the vegetation biomass to the platform elevation z_b with respect to z_{\max} and z_{\min} , namely:

$$b_{ps} = \begin{cases} 0 & z_b < z_{\min} \\ \frac{b_{\max}}{z_{\max} - z_{\min}} (z_{\max} - z_b) & z_{\min} \leq z_b \leq z_{\max} \\ 0 & z_b > z_{\max} \end{cases} \quad (13)$$

where b_{ps} is the biomass as a function of marsh elevation in g/m^2 , and b_{\max} is the maximum biomass.

Furthermore, to account for the seasonal variability in biomass, which usually peaks during the summer months (Morris and Haskin, 1990), the biomass is corrected using the equation:

$$b = \frac{b_{ps}(1-\omega)}{2} \left[\sin\left(\frac{2\pi m}{12} - \frac{\pi}{2}\right) + 1 \right] + \omega b_{ps} \quad (14)$$

with $m = 1, 12$ the month ($m = 1$ corresponds to January) and ω a dimensionless factor that accounts for the reduction in biomass during the winter months (Mudd et al., 2004).

Finally, the fitting of the data collected by Morris and Haskin (1990), indicates that the stem density per unit area, n_s , and the average height of the stems, h_s , can be expressed as a function of plant biomass (Mudd et al., 2004):

$$n_s = \alpha_n b^{\beta_n} \quad (15)$$

$$h_s = \alpha_h b^{\beta_h} \quad (16)$$

where α_n , β_n , α_h and β_h are empirical coefficients.

Analogously, the projected plant area per unit volume, a_s , and the stem diameter, d_s , can be cast as (Mudd et al., 2004):

$$a_s = \alpha_a b^{\beta_a} \quad (17)$$

$$d_s = \alpha_d b^{\beta_d} \quad (18)$$

where α_a , β_a , α_d and β_d are empirical coefficients.

2.4. Simulation setup

Two distinct sets of simulations have been carried out. The first series analyzes how the hydroperiod is influenced by the intertwined interaction between marsh-platform vertical growth and channel formation, and how such processes affect channel cross-sectional evolution, without taking into account for the growth of vegetation on the emerging marshes. The second series analyzes the effect of vegetation on flow resistance, sediment trapping, production of organic soil and,

therefore, on channel formation and cross-sectional evolution. In both cases we assume that the volumetric concentration of sediments transported in suspension, C_0 , is constant across the section and equal to 20 mg/l during the entire tidal cycle.

We consider a tidal sub-basin (see, e.g. Fig. 1), characterized by a cross section of width $B = 200$ m, and a landward length $L = 1000$ m, having therefore a drainage area of 2.0×10^5 m². The initial bottom elevation is $z_{b0} = -1.00$ m below mean sea level (MSL). A forcing semidiurnal sinusoidal tide characterized by a semi-amplitude equal to 0.74 m above MSL is assumed, so that at the beginning of the simulation, the bottom is submerged during the entire tidal cycle. This approach is taken in order to simulate the emergence of a marsh platform from a tidal mud flat. We consider fine cohesive sediments with characteristics reported in Table 1. In particular, since we are interested in the long-term morphological evolution of the marsh cross section, the critical bottom shear stresses for erosion, τ_e , and deposition, τ_d , are those characterizing fully consolidated mud (Pritchard, 2001). Table 1 also shows the values of the parameters necessary to evaluate the various terms in the sediment continuity equation (i.e., Eq. (6)). *Spartina alterniflora* is assumed to be the dominant vegetation species which colonizes the emerged salt-marsh surfaces. In all runs we start from a deep, flat, and unchanneled initial bottom configuration with a small incision (1.0 cm) in correspondence of the longitudinal axis of the computational domain, to favor channel initiation at that location.

3. Model results

The main results of the first series of simulations are shown in Figs. 2–4. Fig. 2 portrays the time evolution of the channel cross-sectional geometry (Fig. 2a) and of the relative distribution of bottom shear stresses (Fig. 2b), together with the time evolution of the bottom elevation in correspondence of the channel axis and of a point located on the salt marsh (Fig. 2c). It clearly appears that, during the initial stages of the morphodynamic evolution, the threshold value for erosion, τ_e , is nowhere exceeded within the cross section (Fig. 2a,b;

Table 1
Parameters used in the simulations

Parameter	Value	Ref.	Parameter	Value	Ref.
τ_e	0.4 N/m ²	Parchure and Mehta (1985)	α_a	0.25	Mudd et al. (2004)
τ_d	0.1 N/m ²	Parchure and Mehta (1985)	β_a	0.5	Mudd et al. (2004)
ρ_s	2600 kg/m ³		α_d	0.0006	Gibbs (1985)
w_s	2×10^{-4} m/s	Gibbs (1985)	β_d	0.3	Fagherazzi and Furbish (2001)
D_{50}	50 μ m		α_n	250	Mudd et al. (2004)
λ	0.4		β_n	0.3032	Mudd et al. (2004)
Q_{e0}	3.0×10^{-4} kg/m ² s	Fagherazzi and Furbish (2001)	α_h	0.0609	Gibbs (1985)
C_0	20 mg/l	Mudd et al. (2004)	β_h	0.1876	Fagherazzi and Furbish (2001)
R	2.0	Mudd et al. (2004)	α_{cd}	0.224	Mudd et al. (2004)
α_η	0.224	Palmer et al. (2004)	c_{d0}	0.718	Mudd et al. (2004)
β_η	0.718	Palmer et al. (2004)	z_{\min}	0.14 m	Morris et al. (2002)
γ_η	2.08	Palmer et al. (2004)	z_{\max}	0.72 m	Morris et al. (2002)

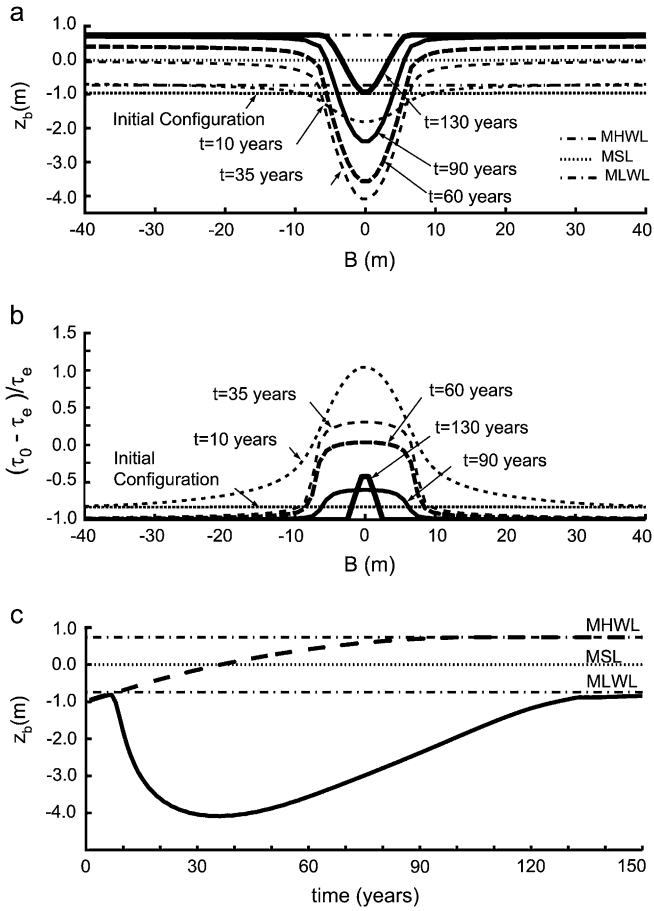


Fig. 2. Evolution in time of (a) cross-sectional bottom elevations and (b) relative distributions of the maximum bottom shear stresses through a tidal cycle, in and near the channel, and evolution in time of (c) the elevation of the channel axis (solid line) and of a point located on the marsh surface (dashed line), in the unvegetated scenario. Mean high water level (MHWL), mean sea level (MSL), and mean low water level (MLWL) are also indicated.

initial configuration). However, the progressive increase in bottom elevation associated to deposition leads to shear stress values greater than τ_e over a part of the cross section, in particular at points closer to the channel axis, where the initial bottom incision is located. A small primary drainage channel characterized by shelving banks develops (Fig. 2a: $t = 10$ years). Flux begins to concentrate within the channel after

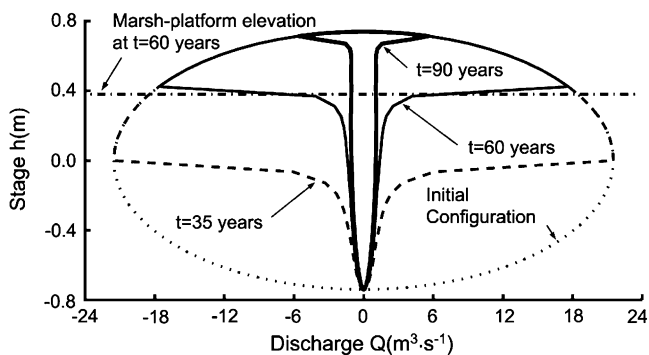


Fig. 3. Stage–discharge relationship during the tidal cycle at different stages of channel development. Mean marsh-platform elevation at $t = 60$ years is also indicated (dash–dot line).

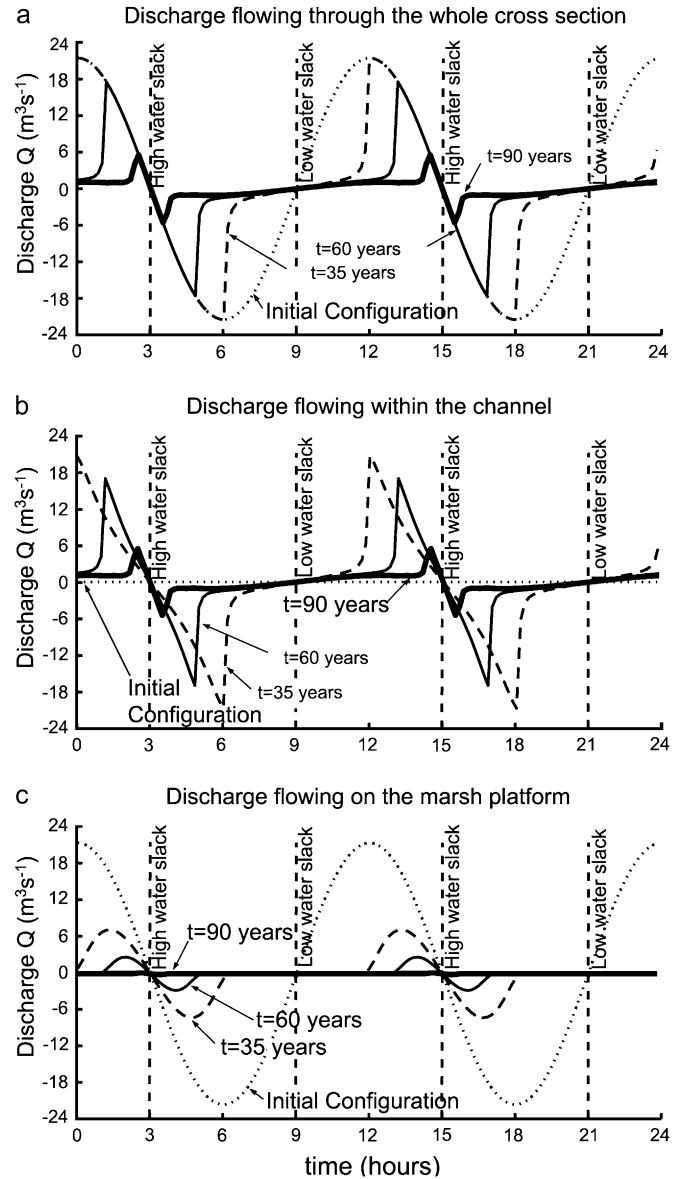


Fig. 4. Discharge–time relationship during the tidal cycle at different stages of channel development. (a) Discharge flowing through the whole cross section; (b) discharge flowing within the channel; (c) discharge flowing on the marsh platform.

its formation due to its increasing cross-sectional area and decreasing flow resistance that is the result of an increase in the depth of flow within the channel. The increased flow velocity associated to the reduction of the relative bottom roughness in the channel with respect to the adjacent marsh platform leads to higher bottom shear stresses and, consequently, to erosion and deepening of the channel, creating a feedback mechanism between erosion and channel formation. On the marsh surface adjacent to the channel, the flow velocity is everywhere decreasing to maintain the discharge equal to the one prescribed by Eq. (1) (Fig. 2b: $t = 10$ years). As channel depth increases, both through bed erosion and by accretion of the adjoining marsh platform, the shelving slopes of the channel are transformed into steeper banks (Fig. 2a: $t = 35$ years). As the marsh platform grows above mean sea level,

a reduction in the maximum discharge is observed as a consequence of the reduction of the tidal prism due to the emergence of part of the tidal sub-basin. Deposition tends to prevail over erosion and the channel starts silting thus increasing its average bed elevation and decreasing its width (Fig. 2a: $t > 35$ years). The shape of the resulting cross section, composed of a high level marsh with a well developed channel, is dictated by the succession of the landscape-forming discharges that the channel has experienced. At the end of the simulation, since the marsh surface is close to high tide level, overbank fluxes are rare and only tidal fluxes confined within the channel prevent its silting. The final channel geometry (Fig. 2a: $t = 130$ years) stems thus from a delicate balance between erosion and deposition.

The above evolutionary scenario is clearly confirmed by Fig. 2c, which shows the time evolution of the bottom elevation in correspondence of the channel axis (solid line) and of a point located on the salt marsh, where erosion is negligibly small (dashed line). It appears that the channel axis deepens as long as the marsh platform lies below mean sea level. As soon as the marsh platform gets higher than mean sea level, two combined processes modify the morphological evolution of the marsh. The reduction in hydroperiod progressively slows deposition over the marsh platform, whose elevation asymptotically tends to mean high water level, in accordance with observational evidence put forth by Pethick (1981). Meanwhile the reduction in tidal prism reduces the tidal discharges in the channel and the related shear stresses, favoring the infilling of the channel.

The reduction of the maximum value attained by the flow discharge during the tidal cycle, when the elevation of the marsh platform becomes higher than mean sea level, is illustrated in Fig. 3, which reports some typical examples of the stage–discharge relationship at different stages of the morphological evolution. When the marsh platform is submerged during the entire tidal cycle, the curve is symmetrical with respect to the mean water level. The drainage area, A , to the considered cross section, in fact, does not vary in time ($B_{\text{wet}} = B$), and maximum flood and ebb discharges occur when dh/dt is maximum or minimum, respectively (i.e., when the water elevation $h = 0$). On the other hand, when the marsh surface emerges, the maximum value of the discharge tends to decrease, the reduction being progressively enhanced as the marsh elevation increases. The maximum flood and ebb discharges are attained when the time derivative of the product $A(t)D_0(t)$ is maximum. The stage–discharge relationship provided by the model qualitatively agrees with observational evidence (e.g., Myrick and Leopold, 1963; Bayliss-Smith et al., 1978; Healey et al., 1981; French and Stoddart, 1992), even if the model, when considering a sinusoidal forcing, cannot capture the asymmetries of such a relationship which are typically observed in tidal landscapes. In particular, for basins with marshlands that fully dry during a tidal cycle, maximum flood discharge occurs after the tide exceeds bank-full elevation and inundates the marsh surface, while, on the contrary, maximum ebb discharge occurs below bank-full elevation (Healey et al., 1981).

Also the shape of the discharge–time curves is influenced by the movement of water across the marsh surface, as shown in Fig. 4 which illustrates discharge–time curves at different stages of the process of channel development. The discharges flowing through the whole cross section (curves in Fig. 4a), within the channel (curves in Fig. 4b), and on the marsh edge (curves in Fig. 4c), all exhibit the typical shape observed in tidal environments (Rinaldo et al., 1999b; Lawrence et al., 2004). If we impose harmonic changes in water elevation as seaward boundary condition and we neglect tidal current asymmetry and distortion, arising from nonlinear effects as the wave propagates from the inlet towards the inner part of the basin, the discharge flowing through the whole cross section (curve relative to the initial configuration in Fig. 4a) is harmonic as well, as long as the elevation of the marsh platform is lower than the minimum water elevation during a tidal cycle (see Eq. (1)). When the elevation of the salt-marsh surface increases due to sedimentation, the bottom topography becomes important and topographic nonlinearities affect the discharge–time relationship, which then loses its harmonic behavior (curves relative to $t = 35, 60$ and 90 years in Fig. 4a). At the beginning of the simulation, when the tidal creek has not yet formed, the discharge flowing through the whole cross section coincides with the discharge flowing on the marsh platform (compare curves relative to the initial configuration in Fig. 4a and c). As the channel develops and the elevation on the marsh platform increases, the discharge is mainly conveyed within the channel (Fig. 4b) and only a small amount of water flows across the marsh platform (Fig. 4c).

The main results of the second series of simulations, taking into account the effects of vegetation, are shown in Figs. 5–9. The evolution in time of the cross-sectional geometry, the stage–discharge relationship and the discharge–time curves are qualitatively similar to those obtained for the unvegetated

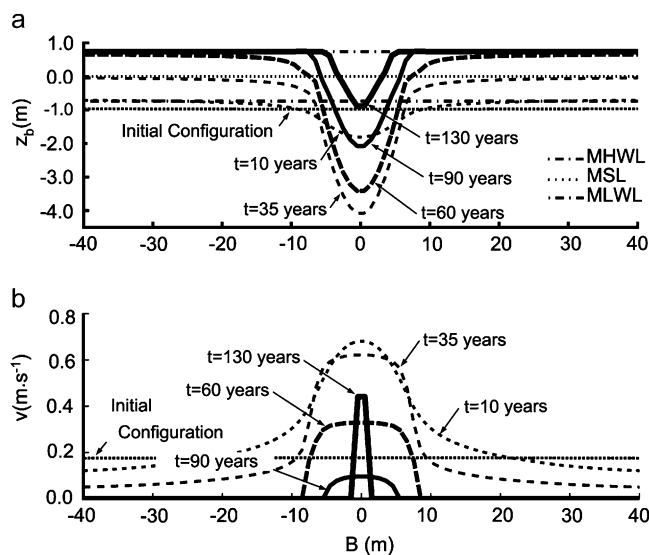


Fig. 5. Evolution in time of (a) cross-sectional bottom elevations and (b) relative distributions of the maximum velocities through a tidal cycle, in and near the channel, in the vegetated scenario.

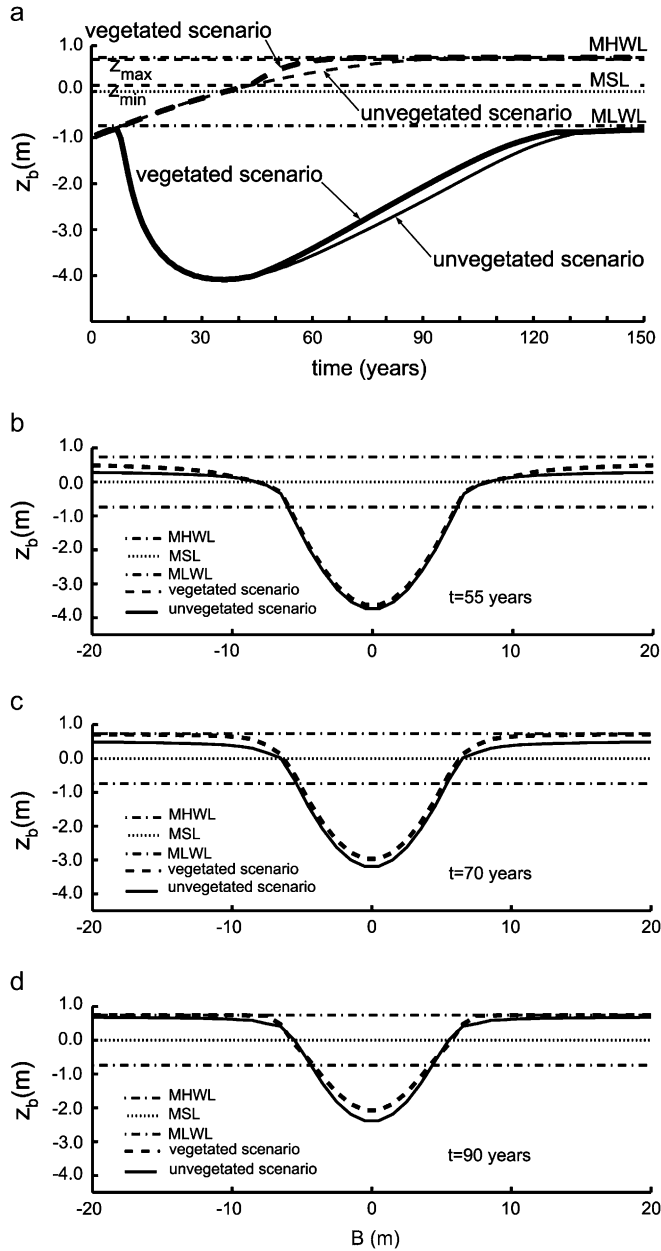


Fig. 6. (a) Comparison of the time evolution of bottom elevation in correspondence of the channel axis (solid lines) and of a point located on the salt marsh (dashed lines), in absence (thin lines) or in presence of vegetation (bold lines); (b,c,d) channel cross sections at different stages of channel development (b: $t = 55$ years; c: $t = 70$ years; d: $t = 90$ years), in the absence (solid lines) or in the presence of vegetation (dashed lines). Mean high water level (MHWL), mean sea level (MSL), and mean low water level (MLWL) are also indicated, together with the vegetation parameters z_{\min} and z_{\max} .

case. Nevertheless, some important differences arise, which need to be discussed. Fig. 5 portrays an example of the time evolution of the cross-sectional geometry (Fig. 5a) and of the relative distribution of maximum flow velocity (Fig. 5b), in the case of a vegetated marsh. As long as the marsh platform is not encroached by vegetation, not surprisingly, cross-sectional bottom configurations (Fig. 5a) show exactly the same behavior as in the unvegetated case (Fig. 2a). However, as soon as vegetation starts populating the marsh surface,

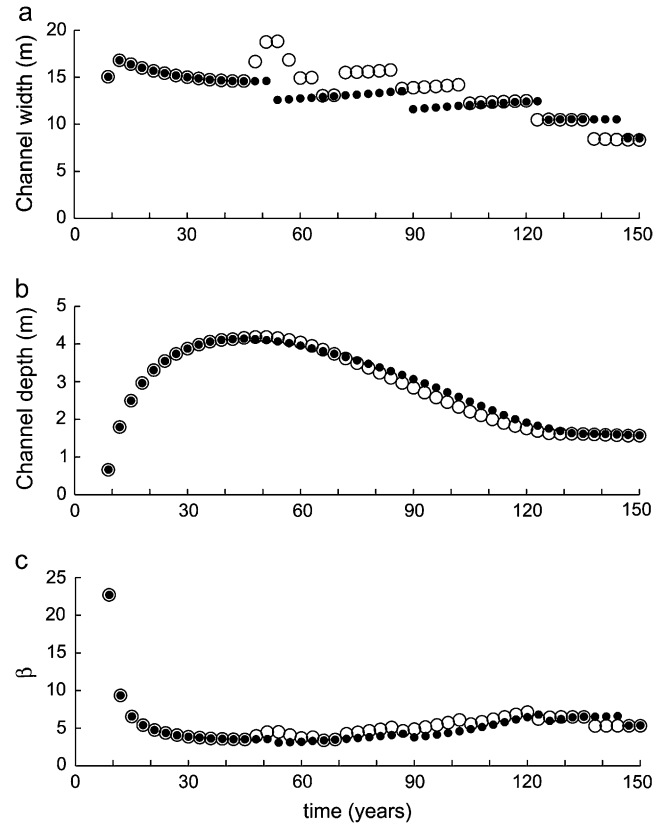


Fig. 7. (a) Channel width, (b) channel depth, and (c) width-to-depth ratio, β , at different stages of channel development, in the absence (solid circles) or in the presence of vegetation (open circles). The channelled portion of the cross section has been evaluated by coupling bed elevation and curvature threshold criteria, in analogy with Fagherazzi et al. (1999). Channel points are those in which $|c| > 0.1 \text{ m}^{-1}$ or $z_{\text{marsh}} - z < 0.3 \text{ m}$, where c and z are, respectively, the curvature and the elevation of the considered point, and z_{marsh} is the average marsh-platform elevation.

it influences both sediment transport processes and flow dynamics. The vertical growth of the marsh platform is enhanced by the increased inorganic sediment deposition due to trapping effects of the canopy and by the deposition of organic sediment (Fig. 5a, $t \geq 35$ years). The velocities on the marsh platform are strongly reduced (Fig. 5b) as well as the discharge flowing on the vegetated part of the cross section. As a consequence, the flow tends to be more concentrated within the channel, increasing the amount of water flowing through it, as to maintain an overall discharge equal to the one prescribed by Eq. (1) (Fig. 5b, $t \geq 35$ years). However, our results suggest that, if vegetation begins to grow when flow velocities on the marsh surface are already very slow, the increased flow within the channel might not be strong enough to modify the section shape (Fig. 5b).

Such an observation is reinforced by Fig. 6. In particular, Fig. 6a shows a comparison of the time evolution of the bottom elevation in correspondence of the channel axis and of a point located on the salt marsh, in the absence or in the presence of vegetation. It clearly appears that vegetation growth modifies the evolution of both the channel bottom and the marsh surface (Fig. 6a). Indeed, the increased deposition rate associated to vegetation trapping and organic

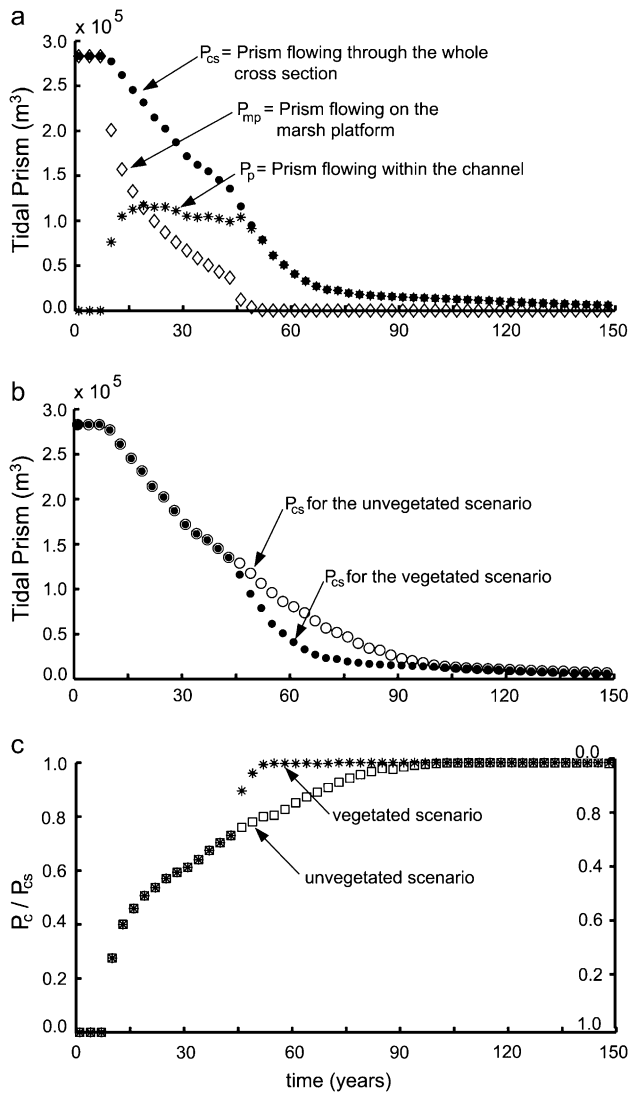


Fig. 8. (a) Repartition of total tidal prism flowing through the whole cross section, P_{cs} in tidal prism flowing within the channel, P_c , and on the marsh platform, P_{mp} estimated through the model at different stages of the evolution. (b) Comparison between P_{cs} values at different stages of the evolution, in the presence or in the absence of vegetation. (c) Comparison between the ratios P_c/P_{cs} and P_{mp}/P_{cs} at different stages of the evolution, in the presence or in the absence of vegetation.

production leads to a faster growth of the marsh platform than in the unvegetated case and, accordingly, to a more rapid reduction in the maximum discharges (see e.g. Fig. 3) which counteracts the “concentration” of discharge within the channel induced by the enhanced resistance on the vegetated areas. Therefore, the channel starts infilling more rapidly, as shown also in Fig. 6b–d, which portrays a comparison between bottom configurations at corresponding stages ($t = 55, 70, 90$ years, respectively), in the unvegetated and vegetated scenarios. Furthermore, it should be noted that in presence of vegetation, the transition between channel banks and adjacent salt-marsh platform tends to become more abrupt.

A comprehensive view of the evolution in time of channel width (evaluated by coupling bed elevation and curvature threshold criteria, in analogy with Fagherazzi et al., 1999),

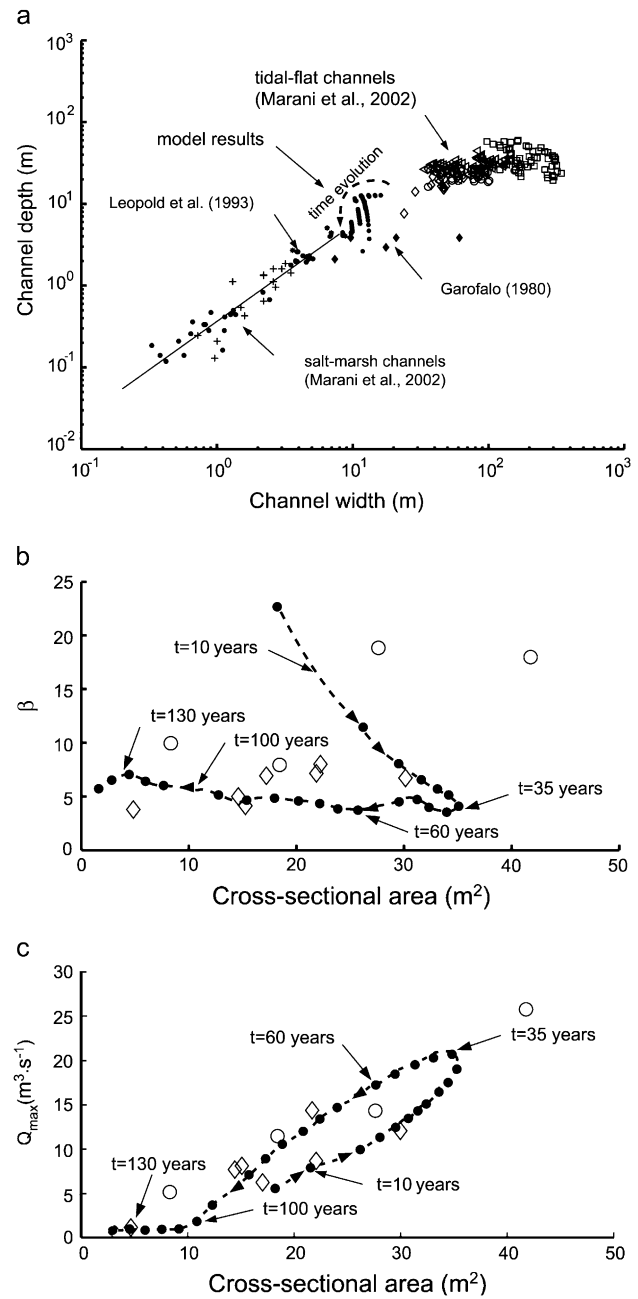


Fig. 9. (a) Calculated channel width versus depth and field data derived from measurements of tidal channels in New Jersey, USA (Garofalo, 1980), San Francisco Bay, USA (Leopold et al., 1993), and in the Venice Lagoon, Italy (Marani et al., 2002). The evolutionary trend of the model results is also shown; (b) evolution in time of the width-to-depth ratio, β , as a function of cross-sectional area, Ω , computed with reference to MSL; (c) evolution in time of maximum flow discharge, Q_{max} , as a function of cross-sectional area, Ω , computed with reference to the MSL. Observed data derived from measurements of tidal channels by Garofalo (1980) (open circles) and Leopold et al. (1993) (diamonds) are also indicated.

channel depth, and width-to-depth ratio, β , is depicted in Fig. 7. Even though the vegetated and unvegetated trends of the above quantities are similar, nonetheless, it emerges that soon after vegetation growth the channel experiences a little widening (Fig. 7a), and, owing to differential accretion, a more pronounced deepening (Fig. 7b). Such an observation

does not contradict the scenario emerging from Fig. 6a–d. In fact, even if the channel infills more rapidly, its depth relative to the marsh surface increases as a consequence of the much faster accretion rate of the adjoining marsh platform (compare channel depth values for the vegetated and unvegetated case in Fig. 7b). The width-to-depth ratio, β , varies in time according to variations in cross-sectional morphology (Fig. 7c). As the channel starts forming within the tidal-flat surface its cross section is characterized by β -values close to 23. A relatively rapid decrease of β characterizes the next stages of channel evolution: channel width, in fact, maintains nearly constant (Fig. 7a), while channel depth increases (Fig. 7b) due to prevailing over erosion. Finally, as the marsh platform emerges and, consequently, the maximum discharges decrease, β tends to slightly increase as a consequence of channel silting which prevails on channel narrowing.

4. Discussion

The static hydrodynamic model described in the previous sections appears to reproduce a geomorphologically relevant feature of tidal creek hydrodynamics, namely the significant decrease in maximum discharges within the channels attained when tide levels are just below the bank-full elevation and the marsh platform dries (see Figs. 3 and 4) in accordance with the field observations carried out by Myrick and Leopold (1963), Bayliss-Smith et al. (1978), Pethick (1980), and Healey et al. (1981). Moreover, despite its simplifying assumptions, the proposed model gives a satisfactory estimate of the tidal discharge for relatively small tidal basins (Lanzoni and Seminara, 1998; Fagherazzi, 2002; Fagherazzi et al., 2003), particularly when the three-dimensional structure of the marsh is unknown. Obviously, some observed features such as the asymmetry of the velocities in the creeks when the marsh platform is inundated/draind, and the delay in the velocity peak after marsh inundation, associated to the strong nonlinearities produced by wetting and drying, cannot be captured by a static model (Healey et al., 1981), which presupposes a flat water surface which moves synchronously with the tidal forcing.

The coupling of the simplified hydrodynamic model with erosion/deposition relationships and a parametrization of vegetation effects make it possible to reproduce evolutionary scenarios which are in accordance with a number of conceptual models depicting the intertwined evolution of tidal channels and the adjoining marsh platform (e.g., Yapp et al., 1916, 1917; Beeftink, 1966; French and Stoddart, 1992; French, 1993; Steel and Pye, 1997). In particular, the different stages of marsh development envisioned by various conceptual models (see the review by Allen, 2000) are reflected in the simulated channel cross-sectional evolution. In the initial stages the topographic irregularities of tidal flats influence the morphology of the forming marsh channels. Indeed, we have shown that even a small perturbation in the tidal-flat bottom triggers the formation of a marsh channel as long as the flow concentration is enough to produce erosion. Intermediate stages of channel evolution typical of youthful marshes, are characterized by a progressive deepening and enlarging of

the channel. During the deepening process the channel cuts older deposits remobilizing the sediments. The channel width is established earlier in the evolution, whereas the depth is more sensitive to discharge variations, as shown in Fig. 7a,b, indicating that channel depth varies in a wider range than channel width. In the final stage the emergence of the marsh platform reduces significantly the tidal discharges in the channel, so that deposition overcomes erosion. During this phase the channel tends to be filled, reducing both its width and depth. At the end of the evolution, when the platform elevation is close to mean high tide level, the contribution of the marsh edge to the total discharge is negligibly small, and the tidal flux is essentially confined to the channel (see e.g., Fig. 4). The repartition of tidal prism between channel and marsh platform along the cross section B–C estimated through the model at different stages of evolution is shown in Fig. 8. When the marsh begins to emerge ($t = 35$ years), most of the discharge is concentrated within the channel, which accounts for 60% of the discharge, in agreement with the numerical results of Lawrence et al. (2004) and the measurements of French and Stoddart (1992) for a U.K. marsh characterized by a mean high water level of 0.8 m (Lawrence et al., 2004), above the marsh platform, i.e., similar to the calculated configuration attained after 35 years. However, Fig. 8a indicates that as the channel further develops and the marsh platform vertically grows, the total tidal prism flowing through the whole cross section decreases and gets more and more concentrated within the channel, while the tidal prism flowing on the marsh surface is strongly reduced.

As far as the effects of vegetation on the tidal prism are concerned, Fig. 8b clearly shows that the reduction in time of the total tidal prism is enhanced by the vegetation encroachment. This is due to the fact that the marsh platform grows more rapidly because of the increased deposition of organic and inorganic sediment. The presence of vegetation, also induces an increase in flow resistance and, therefore, favors the concentration of discharge within the channel. However, as shown in Fig. 8c, in our simulations such an increase is experienced “late” in the process of cross-sectional evolution, i.e., when the maximum discharges shaping the channel have already been considerably reduced (see also Figs. 3 and 4a,b).

Vegetation encroachment on the marsh surface is thus found to produce two competing effects. On the one hand, the increase in flow resistance on the marsh platform concentrates the flow in the channel, leading to a possible channel overdeepening. On the other hand, vegetation also favors deposition of both organic and inorganic material, thus increasing the platform elevation with a reduction in tidal prism and related discharges, resulting in channel infilling. Our simulations suggest that the second process is more important during marsh evolution, because the further concentration of flux within the channel due to vegetation encroachment occurs at a later stage of marsh accretion, when most of the flow is already confined to the channel. Obviously, the situation might be different when vegetation colonizes the surface at lower elevations or when the tidal signal is strong

enough to move large volumes of water on the marsh surface, as it happens in the macrotidal U.K. marshes.

The evolutionary trend exhibited by the width-to-depth ratio, depicted in Fig. 7, suggests that the cross-sectional geometry tends to evolve from an initial configuration typical of tidal-flat channels (characterized by larger values of β) towards a final configuration resembling salt-marsh creeks (characterized by smaller values of β). This behavior is apparent also in Fig. 9a, reporting calculated channel width versus depth values, as well as observed data derived from measurements of tidal channels in *Spartina* marshes in New Jersey (Garofalo, 1980), San Francisco Bay (Leopold et al., 1993), and in tidal flats and salt marshes (with a mix of vegetation species) in the Venice Lagoon, Italy (Marani et al., 2002). All these three environments are characterized by a tidal excursion comparable to the one adopted in our model.

The calculated values not only are compatible with observed features, but also suggest an evolutionary trend according to which both channel width and depth continuously reduce as the intertidal areas flanking the channel progressively grow and become vegetated, transforming the tidal flat into a salt marsh. Such a picture is confirmed by the time evolution of the relationship between β , and the cross-sectional area, Ω , computed with reference to MSL, shown in Fig. 9b. In the early stages of channel development β rapidly decreases while Ω increases until the marsh-platform elevation becomes greater than the MSL. The subsequent reduction of the landscape-forming discharges (see e.g., Fig. 3) then leads to a progressive decrease of the cross-sectional area, which, however, maintains a nearly constant value of β . It might be worthwhile to note that the ranges experienced by β and Ω during the section evolution resulting from our simulation are in agreement with the values typical of observed sections (Garofalo, 1980; Leopold et al., 1993).

Finally, the time evolution of the relationship between peak discharge and cross-sectional area, shown in Fig. 9c, suggests that the average channel velocity remains nearly constant during channel evolution, as long as the marsh platform is significantly lower than mean high water level. The estimated average channel velocity turns out to be roughly 0.5 m/s, a value consistent with field data observations of Garofalo (1980) and Leopold et al. (1993). We can then infer that during the transition from tidal flats to salt marshes, although the channel shape changes in time, reducing its width with respect to the depth, a nearly linear relationship holds between cross-sectional area and peak discharge, thus indicating that the cross section adapts quite rapidly to changes in water discharge.

Further studies are deemed necessary to incorporate important processes acting on salt marshes: time-dependent deposition as a function of platform elevation (Temmerman et al., 2003a); spatial gradient of sedimentation rates that increase the accretion near the channel and produce levees (Woolnough et al., 1995; Mudd et al., 2004; Temmerman et al., 2004); vegetation zonation (Silvestri and Marani, 2004); and bank collapse linked to meander evolution and geotechnical properties of the sediments (Gabet, 1998; Fagherazzi et al., 2004).

5. Conclusions

The model results presented herein are potentially applicable only to microtidal marshes with a uniform *Spartina* canopy. Nonetheless, they provide insights into tidal channel morphology and evolution that are of general interest. The main conclusions of our simulations can be summarized as follows:

- Deposition on tidal flats progressively reduces the water depth and increases the bottom shear stresses, promoting erosion. Topographic irregularities enhance flux concentration at given locations, leading to bottom erosion and the formation of a channel in which the flow further concentrates, thus increasing channel dimensions in a self-sustained process.
- A reduction in hydroperiod after the emergence of the marsh platform causes an infilling of the channel due to the reduced discharge, and an asymptotic growth of the marsh elevation, caused by a decreased deposition rate.
- Vegetation encroachment on the marsh surface produces two competing effects. On the one hand, the increased flow resistance on the canopy promotes the concentration of the flow within the channel, leading to channel over-deepening. On the other hand, enhanced marsh accretion associated to vegetation reduces the tidal prism and the hydroperiod, thus resulting in channel infilling. Our simulations indicate that the second process is more important in microtidal marshes dominated by *Spartina alterniflora*, where the vegetation encroachment occurs when most of the tidal flux is already confined in the channel.
- At the beginning of the simulation the tidal exchanges with the ocean occur as sheet flow on the tidal-flat surface. When the tidal flat emerges and becomes a salt marsh, most of the flow is concentrated within the channel, which accounts for more than 60% of the tidal prism. Finally, in a mature salt marsh (elevation higher than 30 cm above MSL) more than 90% of the tidal prism is confined in the channel. Furthermore the increase in friction driven by vegetation encroachment favors the concentration of flow in the channel.
- The temporal variability of channel depth is higher than the variability of channel width, suggesting that changes in tidal prism most likely produce bottom infilling—scouring rather than channel widening—narrowing. As a consequence, the aspect ratio changes during channel evolution, and, in particular, during the transition from tidal flats to salt marshes.
- The ratio between peak discharge and cross-sectional area (i.e., the maximum average velocity in the channel) remains nearly constant during channel evolution. Therefore, although the shape of the cross section depends on channel history, its area is dictated by the tidal prism and related discharges.

Acknowledgments

Funding from: the Office of Naval Research, award n. N00014-05-1-0071, the Center for Earth Surface Processes

Research (CESPR), Florida State University; the TIDE EU RTD Project (EVK3-2001-00064); 2001 ASI project Dinamica degli ambienti a marea; 2001 MURST 40% Idrodinamica e Morfodinamica a Marea; CORILA (Consorzio per la Gestione del Centro di Coordinamento delle Attività di Ricerca inerenti il Sistema Lagunare di Venezia) (Research Program 2000–2004, Linea 3.2 Idrodinamica e Morfodinamica Linea 3.7 Modelli Previsionali); and Fondazione Ing. A. Gini are gratefully acknowledged.

References

- Allen, J.R.L., 1994. A continuity-based sedimentological model for temperate-zone tidal salt marshes. *Journal of the Geological Society of London* 151, 41–49.
- Allen, J.R.L., 1995. Salt-marsh growth and fluctuating sea level: Implications of a simulation model for Holocene coastal stratigraphy and peat-based sea-level curves. *Sedimentary Geology* 113, 21–45.
- Allen, J.R.L., 1997. Simulation models of salt-marsh morphodynamics: some implications for high-intertidal sediment couplets related to sea-level change. *Sedimentary Geology* 113 (3–4), 211–223.
- Allen, J.R.L., 2000. Morphodynamics of Holocene salt marshes: a review sketch from the Atlantic and Southern North Sea coasts of Europe. *Quaternary Science Review* 19 (17–18), 1155–1231.
- Bayliss-Smith, T.P., Healey, R., Lailey, R., Spencer, T., Stoddart, D.R., 1978. Tidal flows in salt-marsh creeks. *Estuarine and Coastal Marine Science* 9, 235–255.
- Beefink, W.G., 1966. Vegetation and habitat of the salt marshes and beach plains in the south-western part of The Netherlands. *Wentia* 15, 83–108.
- Boon III, J.D., 1975. Tidal discharge asymmetry in a salt marsh drainage system. *Limnology and Oceanography* 20, 71–80.
- Blum, L.K., Christian, R.R., 2004. Belowground production and decomposition along a tidal gradient in a Virginia salt marsh. In: Fagherazzi, S., Marani, M., Blum, L.K. (Eds.), *The Ecogeomorphology of Salt Marshes*. Estuarine and Coastal Studies Series. American Geophysical Union, pp. 47–74.
- Cahoon, D.R., Ford, M.A., Hensel, P.F., 2004. Ecogeomorphology of *Spartina patens*-dominated tidal marshes: soil organic matter accumulation, marsh elevation dynamics, and disturbance. In: Fagherazzi, S., Marani, M., Blum, L.K. (Eds.), *The Ecogeomorphology of Salt Marshes*. Estuarine and Coastal Studies Series. American Geophysical Union, pp. 247–266.
- Christiansen, T., Wiberg, P.L., Milligan, T.G., 2000. Flow and sediment transport on a tidal salt marsh surface. *Estuarine, Coastal and Shelf Science* 50 (3), 315–331.
- D'Alpaos, A., Lanzoni, S., Marani, M., Fagherazzi, S., Rinaldo, A., 2005. Tidal network ontogeny: channel initiation and early development. *Journal of Geophysical Research* 110, F02001. doi:10.1029/2004JF000182.
- Einstein, H.A., Krone, R.B., 1962. Experiments to determine modes of cohesive sediment transport in salt water. *Journal of Geophysical Research* 67 (4), 1451–1461.
- Engelund, F., 1966. Hydraulic resistance of alluvial streams. *Journal of Hydraulic Division, ASCE* 92 (HY 2), 315–326.
- Fagherazzi, S., Bortoluzzi, A., Dietrich, W.E., Adami, A., Marani, M., Lanzoni, S., Rinaldo, A., 1999. Tidal networks 1. Automatic network extraction and preliminary scaling features from digital terrain maps. *Water Resources Research* 35 (12), 3891–3904.
- Fagherazzi, S., Furbish, D.J., 2001. On the shape and widening of salt marsh creeks. *Journal of Geophysical Research* 106 (C1), 991–1005.
- Fagherazzi, S., 2002. Basic flow field in a tidal basin. *Geophysical Research Letters* 29 (8). doi:10.1029/2001GL013787.
- Fagherazzi, S., Wiberg, P.L., Howard, A.D., 2003. Tidal flow field in a small basin. *Journal of Geophysical Research* 108 (C3), 3071. doi:10.1029/2002JC001340.
- Fagherazzi, S., Gabet, E.J., Furbish, D.J., 2004. The effect of bidirectional flow on tidal platforms. *Earth Surface Processes and Landforms* 29, 295–309.
- Fagherazzi, S., Sun, T., 2004. A stochastic model for the formation of channel networks in tidal marshes. *Geophysical Research Letters* 31. doi:10.1029/2004GL020965.
- Friedrichs, C.T., 1995. Stability shear-stress and equilibrium cross-sectional geometry of sheltered tidal channels. *Journal of Coastal Research* 11 (4), 1062–1074.
- French, J.R., Stoddart, D.R., 1992. Hydrodynamics of salt-marsh creek systems – implications for marsh morphological development and material exchange. *Earth Surface Processes and Landforms* 17 (3), 235–252.
- French, J.R., 1993. Numerical-simulation of vertical marsh growth and adjustment to accelerated sea-level rise, North Norfolk, UK. *Earth Surface Processes and Landforms* 18 (1), 63–81.
- French, J.R., Clifford, N.J., Spencer, T., 1993. High frequency flow and suspended sediment measurements in a tidal wetland channel. In: Clifford, N.J., French, J.R., Hardisty, J. (Eds.), *Turbulence: Perspectives on Flow and Sediment Transport*. Wiley, pp. 249–277.
- Gabet, E.J., 1998. Lateral migration and bank erosion in a salt marsh tidal channel in San Francisco Bay, California. *Estuaries* 21 (4B), 745–753.
- Gardner, L.R., Bohn, M., 1980. Geomorphic and hydraulic evolution of tidal creeks on a subsiding beach ridge plain, North-Inlet, Sc. *Marine Geology* 34 (3–4), M91–M97.
- Gardner, L.R., Porter, D.E., 2001. Stratigraphy and geologic history of a south-eastern salt marsh basin, North Inlet, South Carolina, USA. *Wetlands Ecology and Management* 9, 371–385.
- Garofalo, D., 1980. The influence of wetland vegetation on tidal stream migration and morphology. *Estuaries* 3, 258–270.
- Gibbs, R.J., 1985. Estuarine flocs – their size, settling velocity and density. *Journal of Geophysical Research-Oceans* 90 (NC2), 3249–3251.
- Gleason, M.L., Elmer, D.A., Pien, N.C., Fisher, J.S., 1979. Effects of stem density upon sediment retention by salt-marsh cord Grass, *Spartina alterniflora* Loisel. *Estuaries* 2 (4), 271–273.
- Healey, R.G., Pye, K., Stoddart, D.R., Bayliss-Smith, T.P., 1981. Velocity variation in salt marsh creeks, Norfolk, England. *Estuarine, Coastal and Shelf Science* 13, 535–545.
- Kadlec, R.H., 1990. Overland-flow in wetlands – vegetation resistance. *Journal of Hydraulic Engineering – ASCE* 116 (5), 691–706.
- Krone, R.B., 1987. A method for simulating historic marsh elevations. In: Krause, N.C. (Ed.), *Coastal Sediments '87*. American Society of Civil Engineers, New York, pp. 316–323.
- Lanzoni, S., Seminara, G., 1998. On tide propagation in convergent estuaries. *Journal of Geophysical Research* 103, 30793–30812.
- Lawrence, D.S.L., Allen, J.R.L., Havelock, G.M., 2004. Salt marsh morphodynamics: an investigation of tidal flows and marsh channel equilibrium. *Journal of Coastal Research* 20 (1), 301–316.
- Leonard, L.A., Luther, M.E., 1995. Flow hydrodynamics in tidal marsh canopies. *Limnology and Oceanography* 40 (8), 1474–1484.
- Leonard, L.A., Wren, P.A., Beavers, R.L., 2002. Flow dynamics and sedimentation in *Spartina alterniflora* and *Phragmites australis* marshes of the Chesapeake Bay. *Wetlands* 22 (2), 415–424.
- Leopold, L.B., Collins, J.N., Collins, L.M., 1993. Hydrology of some tidal channels in estuarine marshlands near San Francisco. *Catena* 20, 469–493.
- Lopez, F., Garcia, M.H., 2001. Mean flow and turbulence structure of open-channel flow through non-emergent vegetation. *Journal of Hydraulic Engineering – ASCE* 127 (5), 392–402.
- Marani, M., Lanzoni, S., Zandolin, D., Seminara, G., Rinaldo, A., 2002. Tidal meanders. *Water Resources Research* 38 (11), 1225. doi:10.1029/2001WR000404.
- Marani, M., Belluco, E., D'Alpaos, A., Defina, A., Lanzoni, S., Rinaldo, A., 2003. On the drainage density of tidal networks. *Water Resources Research* 39 (2), 105–113.
- Mehta, A., 1984. Characterization of cohesive sediment properties and transport processes in estuaries. In: Mehta, A.J. (Ed.), *Estuarine Cohesive Sediment Dynamics*. Lecture Notes on Coastal And Estuarine Studies, vol. 14. Springer-Verlag, Berlin, pp. 290–315.
- Morris, J.T., Haskin, B., 1990. A 5-yr record of aerial primary production and stand characteristics of *Spartina alterniflora*. *Ecology* 71 (16), 2209–2217.
- Morris, J.T., 1995. The mass balance of salt and water in intertidal sediments: results from North Inlet, South Carolina. *Estuaries* 18, 556–567.

- Morris, J.T., 2000. Effects of sea level anomalies on estuarine processes. In: Hobbie, J. (Ed.), *Estuarine Science: A Synthetic Approach to Research and Practice*. Island Press, Washington, DC, pp. 107–127.
- Morris, J.T., Sundareshwar, P.V., Nietch, C.T., Kjerfve, B., Cahoon, D.R., 2002. Responses of coastal wetlands to rising sea level. *Ecology* 83, 2869–2877.
- Mudd, S.M., Fagherazzi, S., Morris, J.T., Furbish, D.J., 2004. Flow, sedimentation, and biomass production on a vegetated salt marsh in South Carolina: toward a predictive model of marsh morphologic and ecologic evolution. In: Fagherazzi, S., Marani, M., Blum, L.K. (Eds.), *The Ecogeomorphology of Salt Marshes*. Estuarine and Coastal Studies Series. American Geophysical Union, pp. 165–188.
- Myrick, R.M., Leopold, L.B., 1963. Hydraulics geometry of a small tidal estuary. U.S. Geological Survey Professional Papers 422-B, 18 pp.
- Nepf, H.M., 1999. Drag, turbulence, and diffusion in flow through emergent vegetation. *Water Resources Research* 35 (2), 479–489.
- Nepf, H.M., Vivoni, E., 2000. Flow structure in depth-limited, vegetated flow. *Journal of Geophysical Research* 105 (C12), 28547–28557.
- Palmer, M.R., Nepf, H.M., Pettersson, T.J.R., Ackerman, J.D., 2004. Observations of particle capture on a cylindrical collector: implications for particle accumulation and removal in aquatic systems. *Limnology and Oceanography* 49 (1), 76–85.
- Parchure, T.M., Mehta, A.J., 1985. Erosion of soft cohesive sediment deposits. *Journal of Hydraulic Engineering – ASCE* 111 (10), 1308–1326.
- Parker, G., Garcia, M.H., Fukushima, Y., Yu, W., 1987. Experiments on turbidity currents over an erodible bed. *Journal of Hydraulic Research* 25 (1), 123–147.
- Pethick, J.S., 1980. Velocity surges and asymmetry in tidal channels. *Estuarine and Coastal Marine Science* 11, 331–345.
- Pethick, J.S., 1981. Long-term accretion rates on tidal salt marshes. *Journal of Sedimentary Petrology* 51 (2), 571–577.
- Pestrong, R., 1965. The development of drainage patterns on tidal marshes. Stanford University Publications, Geological Sciences (Technical Report 10) 87 pp.
- Phleger, C.F., 1971. Effect of salinity on growth of a salt marsh grass. *Ecology* 52 (5), 908–911.
- Pizzuto, J.E., 1990. Numerical simulation of gravel river widening. *Water Resources Research* 26 (9), 1971–1980.
- Pritchard, D., 2001. Some problems in two-phase flow: intertidal mudflats and low Reynolds number gravity currents. PhD thesis, University of Bristol.
- Pritchard, D., Hogg, A.J., 2003. Cross-shore sediment transport and the equilibrium morphology of mudflats under tidal currents. *Journal of Geophysical Research* 108 (C10), 3313. doi:10.1029/2002JC001570.
- Randerson, P.F., 1979. A simulation model of salt-marsh development and plant ecology. In: Knights, B., Phillips, A.J. (Eds.), *Estuarine and Coastal Land Reclamation and Water Storage*. Saxon House, Farnborough, pp. 48–67.
- Rinaldo, A., Fagherazzi, S., Lanzoni, S., Marani, M., Dietrich, W.E., 1999a. Tidal networks 2. Watershed delineation and comparative network morphology. *Water Resources Research* 35 (12), 3905–3917.
- Rinaldo, A., Fagherazzi, S., Lanzoni, S., Marani, M., Dietrich, W.E., 1999b. Tidal networks 3. Landscape-forming discharges and studies in empirical geomorphic relationships. *Water Resources Research* 35 (12), 3919–3929.
- Silvestri, S., Marani, M., 2004. Salt marsh vegetation and morphology: modeling and remote sensing observations. In: Fagherazzi, S., Marani, M., Blum, L.K. (Eds.), *The Ecogeomorphology of Salt Marshes*. Estuarine and Coastal Studies Series. American Geophysical Union, pp. 5–26.
- Sanderson, E.W., Ustin, S.L., Foin, T.C., 2000. The influence of tidal channels on the distribution of salt marsh plant species in Petaluma Marsh, CA, USA. *Plant Ecology* 146 (1), 29–41.
- Steel, T.J., Pye, K., 1997. The development of salt marsh tidal creek networks: evidence from the UK. In: *Proceedings of the Canadian Coastal Conference*, CCSEA, pp. 267–280.
- Temmerman, S., Govers, G., Meire, P., Wartel, S., 2003a. Modelling long-term tidal marsh growth under changing tidal conditions and suspended sediment concentrations, Scheldt estuary, Belgium. *Marine Geology* 193 (1–2), 151–169.
- Temmerman, S., Govers, G., Wartel, S., Meire, P., 2003b. Spatial and temporal factors controlling short-term sedimentation in a salt and freshwater tidal marsh, Scheldt estuary, Belgium, SW Netherlands. *Earth Surface Processes and Landforms* 28 (7), 739–755.
- Temmerman, S., Govers, G., Meire, P., Wartel, S., 2004. Simulating the long-term development of levee-basin topography on tidal marshes. *Geomorphology* 63, 39–55.
- Webb, J.W., 1983. Soil–water salinity variations and their effects on *Spartina Alterniflora*. *Contributions in Marine Science* 26 (September), 1–13.
- Woolnough, S.J., Allen, J.R.L., Wood, W.L., 1995. An exploratory numerical-model of sediment deposition over tidal salt marshes. *Estuarine, Coastal and Shelf Science* 41 (5), 515–543.
- Yang, S.L., 1998. The role of *Scirpus* marsh in attenuation of hydrodynamics and retention of fine sediment in the Yangtze Estuary. *Estuarine, Coastal and Shelf Science* 47 (2), 227–233.
- Yapp, R.H., Johns, D., Jones, O.T., 1916. The salt marshes of the Dovey Estuary. Part I. Introductory. *Journal of Ecology* 4, 27–42.
- Yapp, R.H., Johns, D., Jones, O.T., 1917. The salt marshes of the Dovey Estuary. Part II. The salt marshes. *Journal of Ecology* 5, 65–103.